Computer-simulation studies of extrinsic defects in $LiNbO_3$ crystals

H. Donnerberg
University of Osnabrück, FB Physik, P. O. Box 4469, D-4500 Osnabrück, Federal Republic of Germany

S. M. Tomlinson
BIOSYM Technologies, 10065 Barnes Canyon Road, San Diego, California 92121

C. R. A. Catlow
Davy Faraday Research Laboratory, Royal Institution, London, W1X 4BS, England

O. F. Schirmer
University of Osnabrück, FB Physik, P. O. Box 4469, D-4500 Osnabrück, Federal Republic of Germany
(Received 5 November 1990)

In this paper we report our results of atomistic-simulation studies concerning the incorporation of impurity ions into $LiNbO_3$ crystals. We show that the incorporation of impurity ions into the $LiNbO_3$ lattice must involve intrinsic defects, which result mainly from the observed Li_2O deficiency in $LiNbO_3$ crystals. Divalent and also trivalent ions are predicted to substitute intrinsically present Nb_{Li}-antisite defects; i.e., these impurities will finally occupy Li sites. For Mg^{2+} incorporation we are able to compare calculated solution mechanisms with experimentally obtained results.

I. INTRODUCTION

$LiNbO_3$ is one of the most important electro-optical materials.[1] However, many of its technologically relevant properties depend strongly upon impurity centers in these crystals. For instance, transition-metal ions, especially iron, have been found to be responsible for the well-known photorefractive effect, i.e., for light-induced refractive index changes in electro-optic crystals.[2] In addition, both the photoconductivity and the photovoltaic current are influenced by the Fe doping of $LiNbO_3$ crystals.[3]

Whereas the photorefractive effect is useful for the storage of volume phase holograms, it is unwanted in optical-waveguide devices. Zhong *et al.*[4] have discovered that this optical damage is strongly reduced in crystal samples grown from a congruent melt containing at least 4.6 mol % MgO. Thus, high Mg dopings can lead to optical waveguides in which light wave fronts are essentially not disturbed. Several physical properties show abrupt changes when the Mg content is raised above this threshold value (e.g., Ref. 5). However, we should note that the same threshold behavior is observed if $LiNbO_3$ crystals with constant Mg concentration but varying [Li]/[Nb] ratios are investigated.[6,7] From this result one can deduce that Mg ions only indirectly influence the threshold behavior by their mode of incorporation, which seems to be correlated with the dominant intrinsic defect structures in $LiNbO_3$. From these observations it is clear that it is necessary to investigate the incorporation modes of extrinsic defects in $LiNbO_3$ crystals. Here the important questions of interest are the site of incorporation and favorable charge compensation mechanisms. The results should be of considerable value in elucidating relationships between the microstructure of defects and their influence on macroscopic properties.

There are only a few experimental investigations concerning the site of impurity ions in the $LiNbO_3$ crystal lattice. From ESR it is known that most impurity ions prefer incorporation at one definite site, probably either a Li or a Nb site. More specific information may be obtained by electron nuclear double resonance (ENDOR) measurements, as in the recent investigations on $LiTaO_3:Fe^{3+}$, a system that is structurally isomorphous to $LiNbO_3:Fe^{3+}$, and on $LiNbO_3:Mn^{2+}$.[8,9] ENDOR can yield the site of incorporation more directly than most other methods, which rely, in almost all cases, on rather indirect evidence. The angular dependences of the ENDOR transitions point to Li-site incorporation for both Fe^{3+} and Mn^{2+}. This is in accord with recent extended x-ray-absorption fine-structure (EXAFS) measurements.[10] However, in the case of Fe^{3+}, we should emphasize that the ENDOR spectrum of $LiTaO_3:Fe^{3+}$ shows, besides the sharp lines belonging to Fe^{3+} in a well-defined lattice site, a large and broad signal which could also be attributed to Fe^{3+}. It may be argued that this latter signal results from interactions of Fe^{3+} with nearby intrinsic defect structures. However, the nature of these additional involved defects is not yet clear.

Computer-simulation techniques based on ionic-shell-model[11] potentials and the Mott-Littleton approximation[12] are able to provide reliable estimates of defect and dopant energies. In a previous paper,[13] we have reported our results on intrinsic defects in $LiNbO_3$ using these techniques. For computational details and for the appropriate potential models describing $LiNbO_3$ in the paraelectric and ferroelectric phases, we refer the reader to that paper. However, in addition to the intrinsic potential models discussed in Ref. 13, short-range potentials between the impurity ion and neighboring oxygen ions,

respectively, are needed. Commonly these interactions are assumed to be of a Born-Mayer type:

$$\Phi_{ij}(r) = A_{ij}\exp(-r/\rho_{ij}) \ . \tag{1.1}$$

The unknown parameters A_{ij} and ρ_{ij} may either be obtained by theoretical methods using, for example, electron-gas procedures[14,15] or by empirical fitting to observed crystal properties of the relevant binary oxides. In the course of our work, both types of potential sets have been investigated; the empirical potential parameters are taken from Ref. 16. However, our results concerning the site of impurity incorporation and charge compensation mechanisms turn out to be independent of this choice of potentials. All energies listed in this paper refer to electron-gas potentials, unless otherwise specified.

II. RESULTS

A. Incorporation and charge compensation of extrinsic defects

We first consider incorporation in perfect stoichiometric $LiNbO_3$. The following incorporation reactions (given in Kröger-Vink notation) for divalent ions M^{2+} represent the most probable of the large number of possible solution mechanisms which obey charge and particle conservation:

$$MO + \text{“}LiNbO_3\text{”} \rightleftharpoons M_{Li}^{\cdot} + V_{Li}' + Li_2O \ , \tag{2.1}$$

$$4MO + \text{“}LiNbO_3 \rightleftharpoons 4M_{Li}^{\cdot} + Li_{Nb}^{4'} + LiNbO_3 + Li_2O \ , \tag{2.2}$$

$$4MO + \text{“}LiNbO_3\text{”} \rightleftharpoons 3M_{Li}^{\cdot} + M_{Nb}^{3'} + LiNbO_3 + Li_2O \ , \tag{2.3}$$

$$2MO + \text{“}LiNbO_3\text{”} \rightleftharpoons 2M_{Nb}^{3'} + 3V_0^{2\cdot} + Nb_2O_5 \ , \tag{2.4}$$

$$5MO + \text{“}LiNbO_3\text{”} \rightleftharpoons 5M_{Nb}^{3'} + V_{Li}' + 4Nb_{Li}^{4\cdot} + LiNbO_3 + 2Li_2O \ . \tag{2.5}$$

The symbol “$LiNbO_3$” stands for $LiNbO_3$ crystal as a whole. Similar reactions may be formulated for ions with other charge states. Equation (2.3) is an example of the self-compensation mechanism. In Table I we have summarized some calculated results using electron-gas potentials for the short-range impurity-oxygen interaction and potential model II (Ref. 13) for the simulation of the $LiNbO_3$ lattice. By inspection of Table I, one finds self-compensation to be energetically favored for all impurity ions and charge states. As a consequence, impurity ions would substitute Li and Nb ions with almost equal concentrations. Again, we emphasize that we obtain qualitatively the same results when using empirical impurity-oxygen short-range potentials instead of electron-gas potentials. Indeed, our finding that self-compensation is the energetically most favorable impurity incorporation mode in the perfectly grown $LiNbO_3$ crystal lattice seems to be very reasonable because of the geometrical similarity of both the Li and the Nb sites.

However, this result is obviously not in agreement with the experimental observations that most impurity ions are incorporated at only one of the above sites. Thus, one has to look for different impurity solution modes which are in agreement with these observations.

An alternative model involves impurity incorporation at structural vacancy (i.e., interstitial) sites, which have been neglected so far. However, calculations show that this incorporation mode is energetically costly and, in ad-

TABLE I. Incorporation energies for extrinsic defects. The values in parentheses refer to the most favorable charge compensators for Li- and Nb-site incorporations, respectively. These energies have to be compared with the incorporation energies for self-compensation. Defect structures resulting from Li_2O deficiency have not been taken into account.

Impurity ion	Site of incorporation	Favored intrinsic charge compensator [solution energy per impurity ion (eV)]		Solution energy (eV) per impurity ion for self-compensation
Fe^{2+}	Li	$Li_{Nb}^{4'}$	(8.1)	7.3
	Nb	$V_0^{2\cdot}$	(9.5)	
Fe^{3+}	Li	$Li_{Nb}^{4'}$	(9.4)	7.3
	Nb	$V_0^{2\cdot}$	(8.3)	
Mn^{2+}	Li	$Li_{Nb}^{4'}$	(7.4)	6.6
	Nb	$V_0^{2\cdot}$	(8.8)	
Mn^{3+}	Li	$Li_{Nb}^{4'}$	(13.8)	11.7
	Nb	$V_0^{2\cdot}$	(12.6)	
Co^{2+}	Li	$Li_{Nb}^{4'}$	(8.5)	7.7
	Nb	$V_0^{2\cdot}$	(9.9)	
Ni^{2+}	Li	$Li_{Nb}^{4'}$	(9.2)	8.4
	Nb	$V_0^{2\cdot}$	(10.6)	
Mg^{2+}	Li	$Li_{Nb}^{4'}$	(2.7)	2.2
	Nb	$V_0^{2\cdot}$	(5.1)	
Ti^{4+}	Li	$Li_{Nb}^{4'}$	(15.2)	11.7
	Nb	$V_0^{2\cdot}$	(12.1)	

dition, is unstable as impurity interstitials displace neighboring Li ions along the c axis into nearby interstitial sites with the impurity being finally located at a Li site.

Thus, we may conclude that it is impossible to achieve consistency between experimental and theoretical results, if defect structures induced by nonstoichiometry are not taken into account. In this context we should notice that all $LiNbO_3$ crystal samples are, to some extent, Li_2O deficient.[17,18]

In our previous publication[13] we found, following a suggestion by Smyth,[19] that Li_2O-deficient ilmenite intergrowths are likely to represent the dominant defect structures in $LiNbO_3$ crystals with compensation by $Nb_{Li}^{4\cdot}$-antisite defects. The ilmenite Li vacancies can be represented in our model as $(Nb_{Li}^{4\cdot}V_{Nb}^{5'})$ defects which, together with the $Nb_{Li}^{4\cdot}$, are the reactants in the impurity solution reactions. The following reactions are examples for divalent impurity ions:

$$3MO+(Nb_{Li}^{4\cdot}V_{Nb}^{5'})+Nb_{Li}^{4\cdot}+Li_{Li}\rightleftharpoons 3M_{Li}^{\cdot}+LiNbO_3\ , \quad (2.6)$$

$$3MO+(Nb_{Li}^{4\cdot}V_{Nb}^{5'})+2Nb_{Nb}\rightleftharpoons 3M_{Nb}^{3'}+2Nb_{Li}^{4\cdot}+LiNbO_3\ , \quad (2.7)$$

$$MO+(Nb_{Li}^{4\cdot}V_{Nb}^{5'})\rightleftharpoons M_{Li}^{\cdot}+2V_{Li}'+Li_2O\ , \quad (2.8)$$

$$5MO+3(Nb_{Li}^{4\cdot}V_{Nb}^{5'})+2Nb_{Li}^{4\cdot}\rightleftharpoons 5M_{Li}^{\cdot}+Nb_2O_5\ , \quad (2.9)$$

$$5MO+Nb_{Li}^{4\cdot}+4(Nb_{Li}^{4\cdot}V_{Nb}^{5'})\rightleftharpoons 5M_{Li}^{\cdot}+5V_{Li}'+LiNbO_3+2Li_2O\ . \quad (2.10)$$

The way Eqs. (2.6)–(2.10) have to be interpreted is that ilmenite intergrowths containing $(Nb_{Li}^{4\cdot}V_{Nb}^{5'})$ and isolated $Nb_{Li}^{4\cdot}$ antisites are dissolved as a result of impurity incorporation. Li vacancies, now occurring within perfect $LiNbO_3$, may occasionally be created as is shown, for example, in (2.8) and (2.10). In Table II we have listed the relevant solution energies for the case of iron impurities. We note that the important result from Table II is the relative energetic ordering of the above solution reactions, whereas the absolute values of the solution energies are very sensitive to the potentials used. Both sets of calculations show that impurity ions prefer the incorporation mode (2.9). A very similar result holds for trivalent ions, e.g., Fe^{3+}, for which we predict the following dominant solution mode:

$$5M_2O_3+4(Nb_{Li}^{4\cdot}V_{Nb}^{5'})+6Nb_{Li}^{4\cdot}\rightleftharpoons 10M_{Li}^{2\cdot}+3Nb_2O_5\ . \quad (2.11)$$

Comparing Eqs. (2.6) and (2.7), we observe that both solution mechanisms only differ by an additional interchange reaction of the form

$$M_{Nb}^{3'}+Nb_{Li}^{4\cdot}\rightleftharpoons M_{Li}^{\cdot}+Nb_{Nb}\ . \quad (2.12)$$

Similar reactions may also be formulated for impurity ions with different charge states. Thus, in general, the impurity ion site occupancy in Li_2O-deficient $LiNbO_3$ depends upon the energetics of reactions such as (2.12).

The analysis of interchange reactions shows that divalent and trivalent ions will, in every case, prefer Li-site incorporation. This result has been obtained by considering, in (2.12), both isolated $Nb_{Li}^{4\cdot}$ antisites and $Nb_{Li}^{4\cdot}$ with nearby $(Nb_{Li}^{4\cdot}V_{Nb}^{5'})$ defects. These latter defect complexes are likely to occur in Li_2O deficient ilmenite intergrowths. However, calculations of the same type for Ti^{4+} ions do not yield conclusive results. Using isolated $Nb_{Li}^{4\cdot}$ in reaction (2.12), Ti^{4+} ions are seen to be incorporated on Li sites, whereas Nb-site incorporation is favored in the case of reaction with defect complexes.

TABLE II. Incorporation energies (eV) of Fe^{2+} ions into $LiNbO_3$ crystals: stoichiometry-dependent defects are considered. a denotes electron-gas potentials and b denotes empirical potentials in simulating the impurity-oxygen interaction.

Solution reaction	a	b
(2.6)	4.22	−3.77
(2.7)	8.22	0.93
(2.8)	4.97	−3.02
(2.9)	2.29	−5.70
(2.10)	3.60	−4.39

In summary, we may conclude that divalent and trivalent impurity ions prefer Li-site incorporation simply by replacement of the $Nb_{Li}^{4\cdot}$ antisites induced by deviation from stoichiometry. The situation is not as clear for M^{4+} ions, where both solution modes are possible.

Finally, we note the above calculated impurity solution mechanisms are strictly valid only for small impurity concentrations because *single* defect energies have been combined to yield reaction energies. For the usual impurity concentrations in $LiNbO_3$, this approximation is reasonable. However, deviations from these predictions may be expected in the case of Mg^{2+} incorporation, where concentrations of several at. % are observed.

B. Comments on the incorporation of Mg^{2+} ions

As outlined in the previous section, we expect, at least for low Mg concentrations in $LiNbO_3$, Eq. (2.9) to govern the incorporation of Mg, i.e.,

$$5MgO+3(Nb_{Li}^{4\cdot}V_{Nb}^{5'})+2Nb_{Li}^{4\cdot}\rightleftharpoons 5Mg_{Li}^{\cdot}+Nb_2O_5\ .$$

This solution reaction may be used to calculate the Li_2O content of $LiNbO_3$ crystals as a function of Mg doping assuming, as a first guess, reaction (2.9) to be valid over the Mg solution range as far as possible. Figure 1 shows the resulting curve (dash-dotted) together with the experimentally determined dependence.[17] The deviations between experimental points and the dash-dotted curve between 3 and 4 mol % Mg content are clearly seen to exceed the reported margin of experimental error of about 0.5 mol % (with respect to $[Li_2O]$). Thus, reaction (2.9) cannot properly describe the Mg incorporation over its whole solution range. However, it is observed that both dependences agree excellently for Mg doping up to about 1 mol %. Therefore, in the following we assume Eq. (2.9) to be the proper solution mechanism for Mg concentrations less than 1 mol %. For larger Mg concen-

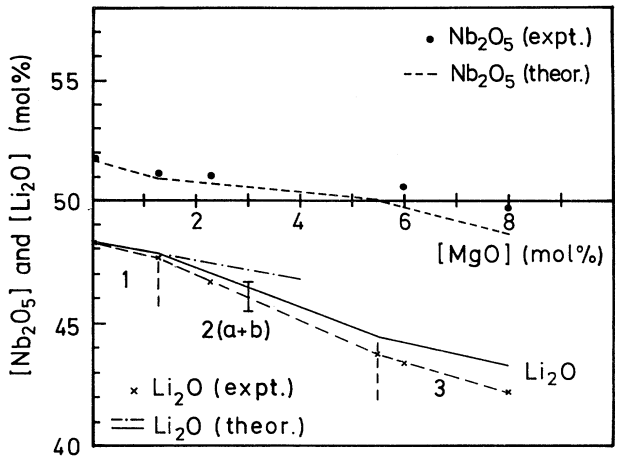

FIG. 1. The theoretical Li_2O and Nb_2O_5 concentrations in $LiNbO_3$ crystals are shown as functions of the MgO concentration. The initial composition is given by the respective experimental value $[Li_2O]=48.3$ mol %. The dash-dotted curve corresponds to the Li_2O-MgO dependence according to reaction 1 only, whereas the solid curve has been obtained using Eqs. (1)–(4). The theoretical Nb_2O_5 dependence corresponds to this latter model too. The relevant reactions are denoted in their corresponding regimes.

trations (>1 mol %) we are then able to extrapolate our calculated results properly, if we use a set of different solution mechanisms, which we choose according to following basic assumptions.

(1) As far as possible, Mg substitutes for antisite Nb ions; i.e., isolated $Nb_{Li}^{4\cdot}$ and $(Nb_{Li}^{4\cdot}V_{Nb}^{5'})$ defects are replaced by Mg ions.

(2) Incorporation mechanisms are chosen to be consistent with experimental observations and should be energetically favorable as extrapolated from CASCADE calculations. Again we emphasize that these CASCADE results are strictly valid only for low Mg concentrations.

Consequently, we obtain the following order of incorporation mechanisms:

(1)

$$5MgO+3(Nb_{Li}^{4\cdot}V_{Nb}^{5'})+2Nb_{Li}^{4\cdot}\rightleftharpoons 5Mg_{Li}^{\cdot}+Nb_2O_5 .$$

(2a)

$$5MgO+4(Nb_{Li}^{4\cdot}V_{Nb}^{5'})+Nb_{Li}^{4\cdot}\rightleftharpoons 5Mg_{Li}^{\cdot}+5V_{Li}'+LiNbO_3+2Li_2O .$$

(2b)

$$MgO+(Nb_{Li}^{4\cdot}V_{Nb}^{5'})\rightleftharpoons Mg_{Li}^{\cdot}+2V_{Li}'+Li_2O .$$

(3)

$$3MgO+V_{Li}'\rightleftharpoons 2Mg_{Li}^{\cdot}+Mg_{Nb}^{3'}+LiNbO_3 .$$

(4)

$$4MgO\rightleftharpoons 3Mg_{Li}^{\cdot}+Mg_{Nb}^{3'}+LiNbO_3+Li_2O .$$

Table III summarizes our calculated solution energies. The respective theoretical curve taking all these reactions into account is given by the solid line in Fig. 1. From Eq. (1) it is observed that the natural ratio

$$[Nb_{Li}^{4\cdot}V_{Nb}^{5'}]:[Nb_{Li}^{4\cdot}]=4:1$$

(see Ref. 13) becomes disturbed with increasing Mg content. For example, a Mg concentration of 1.2 mol % actually results in

$$[Nb_{Li}^{4\cdot}V_{Nb}^{5'}]:[Nb_{Li}^{4\cdot}]=5.8:1 .$$

In Ref. 13 we have argued that Li-deficient ilmenite-like defect clusters are probably the dominant defect structures in $LiNbO_3$. One may think that a drastic change of the above ratio destabilizes the ilmenite intergrowths and thus causes reactions (2a) and (2b) to become preferred because of energetic and/or kinetic reasons. However, this explanation is, of course, unproved because the possible transition from solution mode (1) to solution mode (2) as a result of many defect interactions is beyond the validity range of our performed CASCADE calculations. However, by fitting this transition point to the experimental data (i.e., it should occur close to 1.2 mol % Mg content in congruent $LiNbO_3$ crystals) it is inferred from Fig. 1 that both experimental and theoretical curves agree reasonably well; in particular, the considerable decrease of the Li_2O content between 1.2 and about 6 mol % Mg can be sufficiently well reproduced using reactions (2a) and (2b) in this regime. In addition, the analysis of all possible solution reactions has shown that the creation of Li vacancies as in (2a) and (2b) must be included if the observed slope close to -1.0 is to be described. One may conclude that this Li_2O-MgO relationship depends strongly on the defect model for Mg incorporation as these have different chemical implications.

So far we have explained the incorporation of Mg ions by substitution of intrinsic Nb_{Li} antisites; and there are experimental investigations which are able to support our interpretation. For example, it has been found that an increasing Mg content leads to a pronounced hardening of the $LiNbO_3$ crystal lattice as can be inferred from the observed blueshift of the fundamental absorption. Moreover, phonon frequencies are seen to increase with growing Mg doping.[20,21] On the other hand it is known from the careful x-ray analysis of Abrahams and Marsh[22] that Nb_{Li}-antisite defects behave as soft spots within the $LiNbO_3$ lattice. Thus, it is plausible to assume the lattice har-

TABLE III. Solution energies for Mg^{2+} ions (eV).

Reaction	Reaction energy per Mg ion (eV)
(1)	−2.44
(2a)	−1.12
(2b)	+0.25
(3)	+2.18
(4)	+2.84

hardening to be a consequence of the consumption of Nb_{Li} antisites. In this way, Mg ions are seen to influence $LiNbO_3$ crystal properties, such as the photorefractive effect, by affecting the Nb_{Li}-antisite content. Consequently, it is not the absolute Mg concentration which is physically significant, but the ratio $[Mg]/[Nb_{Li}]$ or, alternatively, $[Mg]/[Li_2O]$.

From Fig. 1 one observes a second transition point occurring between 5 and 6 mol % Mg content if the initial Li to Nb stoichiometry corresponds to the congruent composition. In contrast to the first transition point, this one is well defined, i.e., by the complete absence of misplaced Nb ions. It is worth noting that the disappearance of Nb_{Li}-antisite defects has been suggested to be responsible for the well-known threshold effects observed around 6 mol % Mg concentration in congruent $LiNbO_3$ crystals.[20,21] To complete our discussion we stress that both transition points mentioned above depend on the initial Li_2O content of the $LiNbO_3$ crystals investigated. The lower the Li_2O concentration, the more both transition points are shifted to higher Mg concentrations. Beyond the threshold Mg content we predict solution model (3) to become dominant, thus Mg ions are incorporated on both Li and Nb sites. Reaction (3) may therefore be regarded as being a precursor of the self-compensation mode (4).

Li vacancies created within regime (2) are now used to incorporate Mg ions. The initially increasing vacancy content should therefore be diminished if solution mode (3) comes to the fore. This theoretical expectation is confirmed by the results of a chemical composition analysis,[23] which are shown in Fig. 2.

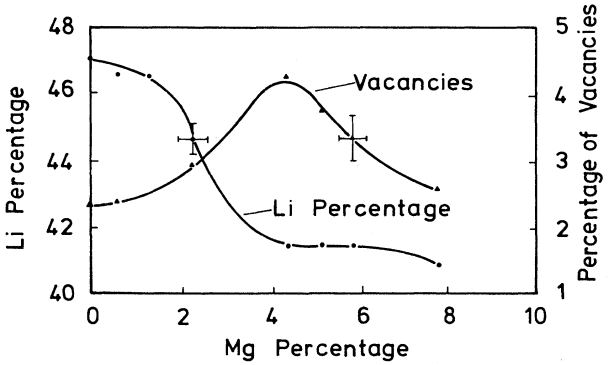

FIG. 2. Percentage of Li^+ ions and vacancies on regular cation sites as functions of the Mg concentration (Ref. 23).

The final Mg solution mode is given by the self-compensation reaction (4). Investigations of the Li_2O-Nb_2O_5-MgO phase diagram[24] (see Fig. 3) have shown the existence of the compound $Mg_4Nb_2O_9$, which has a similar crystal structure to $LiNbO_3$. We stress that the growth of this compound from $LiNbO_3$ may easily be understood given the occurrence of self-compensation. To this end we start with a Mg concentration in $LiNbO_3$ of the order of 18–20 mol %, where all intrinsic defects as described by the above reactions (1)–(3) are dissolved. Thus, up to 25 mol % Mg, the Mg solution limit in $LiNbO_3$, self-compensation is assumed to govern Mg incorporation. Reformulation of reaction (4) yields

$$3LiNbO_3(\equiv Li_3Nb_3O_9)+4MgO\rightarrow[(Mg_{Li}^{\cdot})_3Mg_{Nb}^{3'}](Nb_{Nb})_2O_9+LiNbO_3+Li_2O\rightleftharpoons Mg_4Nb_2O_9+LiNbO_3+Li_2O\ .$$

We finally note that the compound $MgNb_2O_6$ occurring at the Li_2O-deficient site in the phase diagram can be similarly explained using reaction (2a):

$$5MgO+[(Li_{Li}Nb_{Li}^{4\cdot})_5(Nb_{Nb})_6(V_{Nb}^{5'})_4O_{30}]\rightarrow(V_{Li}'Mg_{Li})_5(Nb_{Nb})_{10}O_{30}+LiNbO_3+2Li_2O$$
$$\rightleftharpoons 5MgNb_2O_6+LiNbO_3+2Li_2O\ ,$$

where the material in square brackets is $10LiNbO_3(Li_2O$ deficient).

We conclude this section by considering some aspects of the codoping of $LiNbO_3$:Mg crystals with Fe ions. Although we are not able to present exact results because the relative energies of different incorporation modes of the investigated ions turns out to be rather sensitive to the potential models used, we may predict some trends that are consistent with experimental results. ESR experiments on $LiNbO_3$:Mg, Fe,[25,26] have shown the existence of a second Fe^{3+} signal, in addition to the usually observed one, if the Mg concentration becomes greater or equal to 5–6 mol %. Both Fe^{3+} ESR spectra are found to be axially symmetric without any reduction of point symmetry. Thus, one may think the Fe ions to be located on two different regular lattice sites. This finding can consistently be explained under the assumption that the incorporation of Mg is preferred compared to that of Fe ions, which is in agreement with the result from our impurity potential set based on the electron-gas method. Thus, we may develop the following scenario: The favored incorporation of Mg ions leads to a consumption of all misplaced Nb ions as described by the reactions (1)–2(b). Further doping *must* consequently involve solution reactions of the self-compensation type (including possible precursor reactions). In the case of Fe codoping, these read as

$$Fe_2O_3\rightleftharpoons Fe_{Li}^{2\cdot}+Fe_{Nb}''+LiNbO_3 \qquad (2.13)$$

or

$$5Fe_2O_3+4V_{Li}'\rightleftharpoons 4Fe_{Li}^{2\cdot}+6Fe_{Nb}''+3Nb_2O_5\ . \qquad (2.14)$$

Either way, Fe^{3+} ions are found to be on both the Li and the Nb sites in $LiNbO_3$ for high Mg doping. Thus, from this point of view, the second Fe ESR signal should be ascribed to Fe_{Nb}'' centers.

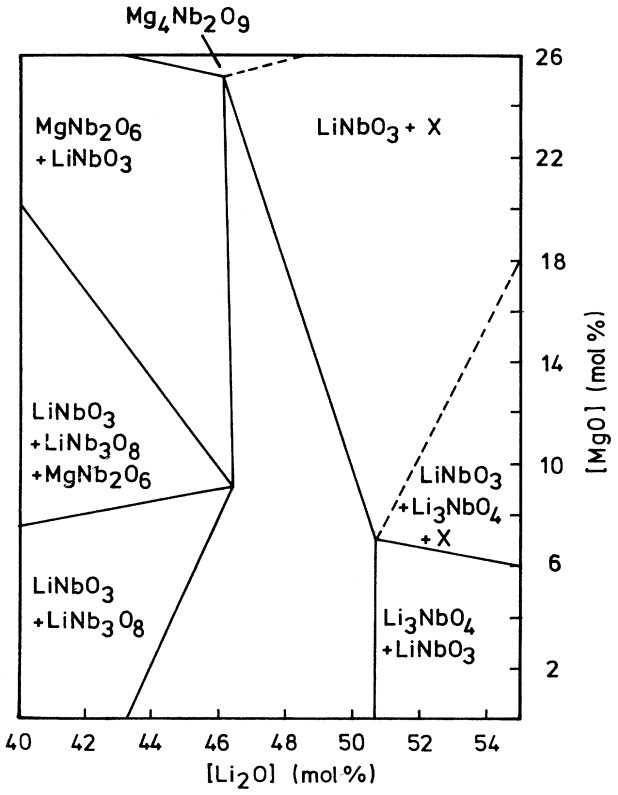

FIG. 3. Li_2O-Nb_2O_5-MgO phase diagram (Ref. 24).

III. CONCLUSIONS

Our previously described treatment of $LiNbO_3$ crystals and the intrinsic defect structures therein using the CASCADE computer code has now been extended to model the incorporation of impurity ions. One important result of our calculations is that all impurity ions prefer the so-called self-compensation solution mode, provided that the presence of defect structures related to the Li_2O deficiency is neglected. As a consequence, impurity ions would substitute Li and Nb ions with almost equal concentrations; this contradicts, however, all experimental experience. The discrepancy between theory and experiment can only be resolved by taking the defect structure due to stoichiometry deviations into account. This leads to the predictions that at least divalent and trivalent impurity ions favor incorporation by replacing intrinsically present $Nb_{Li}^{4.}$-antisite defects. These types of impurity ions therefore prefer Li sites according to our calculation. Moreover, it seems plausible to assume that the incorporation site of impurity ions is frequently rather close to that of the intrinsic defect clusters. Accordingly, one may propose that the broad ENDOR bands in the case of $LiTaO_3$:Fe^{3+} stem from certain interactions between the impurity ions and the ilmenite-like defect clusters. We do not, however, understand why these broad ENDOR bands are absent for $LiNbO_3$:Mn^{2+}. Unfortunately, our calculations are not able to allow definite conclusions in the case of tetravalent impurity ions.

All our defect calculations are strictly valid only for small defect concentrations because single defects have been considered. Deviations from our predictions may be expected if the impurity concentration is of the order of some percent. Mg and Ti dopings are well-known examples where this should be the case. Under some physically plausible assumptions we were able to extrapolate our calculations in order to describe Mg incorporation over the whole solution range. Our results are seen to be in qualitative agreement with chemical analysis. In particular, the well-known threshold phenomena coincide within our model with a disappearance of stoichiometry related defects, which are completely consumed during Mg solution. Above the threshold concentration, Mg ions enter Li as well as Nb sites by means of self-compensation related reactions. Finally, we have tried to give an outline of the impurity incorporation for $LiNbO_3$:Mg codoped with iron. It seems consistent to ascribe a second Fe^{3+} ESR spectrum, which is observable if the Mg concentration exceeds the threshold concentration, to Fe'_{Nb} defects.

[1]A. M. Glass, Science **222**, 657 (1984).
[2]A. Räuber, in *Current Topics in Materials Science,* edited by E. Kaldis (North-Holland, Amsterdam, 1978), Vol. 1.
[3]E. Krätzig, and R. Orlowski, Ferroelectrics **27**, 241 (1980).
[4]G. G. Zhong, J. Jin, and W. Zhong Kang (unpublished).
[5]O. F. Schirmer, O. Thiemann, and M. Wöhlecke, J. Phys. Chem. Solids **52**, 185 (1991).
[6]K. L. Sweeney, L. E. Halliburton, D. A. Bryan, R. R. Rice, R. Gerson, and H. E. Tomaschke, J. Appl. Phys. **57**, 1036 (1985).
[7]F.Klose, M. Wöhlecke, and S. Kapphan, Ferroelectrics **92**, 181 (1989).
[8]H. Söthe, L. G. Rowan, and J.-M. Spaeth, J. Phys.: Condens. Matter **1**, 3591 (1989).
[9]G. Corradi, H. Söthe, and J. M. Spaeth (private communication).
[10]C. R. A. Catlow, G. N. Greaves, and A. V. Chadwick (unpublished).
[11]B. G. Dick and A. W. Overhauser, Phys. Rev. **112**, 90 (1958).
[12]N. F. Mott and M. J. Littleton, Trans. Faraday Soc. **34**, 485 (1938).
[13]H. Donnerberg, S. M. Tomlinson, C. R. A. Catlow, and O. Schirmer: Phys. Rev. B **40**, 11 909 (1989). Note a correction to this paper—**40**, 11 910(E) (1989): The space groups are $R3c(C_{3v}^6)$ in the case of ferroelectric $LiNbO_3$ and $R\bar{3}c(D_{3d}^6)$ in the paraelectric phase.
[14]G. V. Lewis, Ph.D. thesis, University College, London, 1984.
[15]R. G. Gordon and Y. S. Kim, J. Chem. Phys. **56**, 3122 (1972).
[16]G. V. Lewis and C. R. A. Catlow, J. Phys. C **18**, 1149 (1985).
[17]B. C. Grabmaier (unpublished).
[18]A. Mehta, Ph.D. thesis, Lehigh University, Bethlehem, PA 1989.

[19]D. M. Smyth, ISAF 1986, Proceedings of the Sixth IEEE International Symposium on Applications of Ferroelectrics, Bethelehem, PA, p. 115.
[20]K. Polgár, L. Kovács, J. Földvári, and J. Cravero, Solid State Commun. **59**, 375 (1986).
[21]J. Kopptiz, A. J. Kuznetsov, O. F. Schirmer, M. Wöhlecke, and B. C. Grabmaier, Ferroelectrics **92**, 233 (1989).
[22]S. C. Abrahams and P. Marsh, Acta Crystallogr. **42**, 61 (1986).
[23]B. C. Grabmaier (unpublished).
[24]B. C. Grabmaier and F. Otto, J. Cryst. Growth **79**, 682 (1986).
[25]A. Böker, H. Donnerberg, and O. F. Schirmer, J. Phys.: Condens. Matter **2**, 6865 (1990).
[26]H. Feng, J. Wen, H. Wang, S. Han, and Y. Xu, J. Phys. Chem. Solids **51**, 397 (1990).